CHANDRA SAMPLE OF GALAXY CLUSTERS AT Z = 0.4 − 0.55:
EVOLUTION IN THE MASS-TEMPERATURE RELATION

O. K   [1,2]   A. V   [2,1]
To be submitted to ApJ Letters

ABSTRACT

We present spatially-resolved analysis of the temperature and gas density profiles in 6 relaxed galaxy clusters at $z = 0.4 − 0.54$ using long-exposure *Chandra* observations. We derived the total cluster masses within the radius r_{500} assuming hydrostatic equilibrium but without assuming isothermality of the intracluster gas. Together with a similar study based on the *XMM-Newton* observations (Kotov & Vikhlinin), we obtained the mass and temperature measurements for 13 galaxy clusters at $0.4 < z < 0.7$ spanning a temperature interval of $3\,\mathrm{keV} < T < 14\,\mathrm{keV}$. The observed evolution of the $M − T$ relation, relative to the low-redshift references from the *Chandra* sample of Vikhlinin et al., follows $M_{500}/T^{3/2} \propto E(z)^{-\alpha}$, where we measure $\alpha = 1.02 \pm 0.20$ and $\alpha = 1.33 \pm 0.20$ for the spectroscopic and gas mass-weighted temperatures, respectively. Both values are in agreement with the expected self-similar evolution, $\alpha = 1$. Assuming that the cluster mass for given temperature indeed evolves self-similarly, the derived slopes, γ, of the high-redshift $M − T$ relation, $E(z)M_{500} \propto T^\gamma$, are $\gamma = 1.55 \pm 0.14$ for T_{spec} and $\gamma = 1.65 \pm 0.15$ for T_{mg}. Our results show that both the shape and evolution of the cluster $M − T$ relation at $z \simeq 0.5$ is close to predictions of the self-similar theory.

Subject headings: galaxies: clusters: general — surveys — X-rays: galaxies

1. INTRODUCTION

Scaling relations between the cluster parameters such as total mass, average gas temperature, and X-ray luminosity can be used for studying galaxy clusters and their cosmological applications (see Voit 2005 for a recent review). Several recent *Chandra* and *XMM-Newton* studies provide accurate measurements for the $M − T$ relation in low-redshift clusters (Vikhlinin et al. 2005b; Arnaud et al. 2005). While studying the scaling relations for low-redshift clusters allows to address many interesting questions, the knowledge of the evolution of the scaling relations at $z > 0$ is required in many cosmological applications. The X-ray cluster mass measurements based on application of the hydrostatic equilibrium equation (Mathews 1978; Sarazin 1988) rely on observations of the cluster temperature and brightness profiles at large radii. These are technically challenging observations, especially for distant clusters. In the past, the mass measurements for distant clusters were often derived assuming $T(r) = \mathrm{const}$ (e.g., Ettori et al. 2004; Maughan et al. 2005). However, this assumption can significantly bias the mass measurements (Markevitch & Vikhlinin 1997; Maughan et al. 2005).

The first systematic study of the high-redshift cluster $M − T$ relation based on the spatially-resolved temperature profiles to $r \approx r_{500}$ (r_{500} is defined as a radius corresponding mean overdensity $\Delta = 500$ relative to the critical density at a cluster redshift) from the *XMM-Newton* observations was presented in Kotov & Vikhlinin (2005). In this *Paper*, we expand this work by analysing *Chandra* observations for 6 clusters at $z = 0.4 − 0.54$. All our clusters belong to a sample of luminous, dynamically relaxed systems used by Allen et al. (2004) for f_{gas} measurements. Statistical accuracy of the observations from our sample allows us to trace the surface brightness and temperature profiles nearly to r_{500}. *Chandra*'s superb angular resolution minimizes the systematic uncertainties in the spatially-resolved analysis. We use the derived gas density

and temperature profile measurements to infer the total cluster masses and the average temperatures. A combination of the *Chandra* and *XMM-Newton* distant cluster samples provides an accurate determination of the shape and evolution of the cluster $M − T$ relation at $z \simeq 0.5$.

All distance-dependent quantities are derived assuming the $\Omega_M = 0.3$, $\Omega_\Lambda = 0.7$ cosmology with the Hubble constant $H_0 = 72\,\mathrm{km\ s^{-1}\ Mpc^{-1}}$. Statistical uncertainties are quoted at 68% CL.

2. OBSERVATIONS AND DATA REDUCTION

In present analysis, we used the archived *Chandra* observations of $z > 0.4$ clusters. We selected only those objected with the *Chandra* exposures sufficient for temperature measurements to $r \sim r_{500}$. We also selected clusters which appear dynamically relaxed in their *Chandra* images. The selected clusters are listed in Table 1.

Our *Chandra* data reduction follows the procedure described in Vikhlinin et al. (2005a,b). This involves generation of the spatially dependent effective area and detector response files, modeling of the particle-induced detector background following Markevitch et al. (2003), and subtraction of the residual Galactic foreground as described in Vikhlinin et al. (2005a).

All detectable point and small-scale extended sources were masked out from the analysis of azimuthally averaged surface brightness and temperature profiles. The sources were detected using a wavelet decomposition technique described in Vikhlinin et al. (1998). The sources were automatically detected in the 0.7–2 keV and 2–7 keV energy bands and the merged region mask was checked manually.

All visible large-scale extended X-ray sources were also excluded from the data. Such structures are present in 3 clusters. In MACSJ0159.8-0849 there are detectable filamentary structures with a size of $\sim 2'$, located at $\simeq 5'$ from the cluster center (at RA = 30.031°; Dec = −8.854° and RA = 29.965°; Dec = −8.921°). MACSJ1621.3+3810 is projected on the outskirts of a low-redshift galaxy group ($\sim 25'$ from the group center). The X-ray emission associated with the group is clearly

[1] Space Research Institute, Moscow, Russia; kotov@head.cfa.harvard.edu
[2] Harvard-Smithsonian Center for Astrophysics, 60 Garden St., Cambridge, MA 02138

TABLE 1

		B	F P		G D	P		R	S	M	D	
Cluster	z	n_{02}/n_0[a]	r_c[a] (kpc)	r_s[a] (kpc)	α[a]	β[a]	ε[a]	r_{c2}[a] (kpc)	β_2[a]	r_{500} (kpc)	T_{spec} (keV)	T_{mg} (keV)	M_{500} ($10^{14} M_\odot$)
MACS1423.8+2404 .	0.539	14.9	28	1220	1.86	0.53	4.94	0.02	1.00	973 ± 72	7.02 ± 0.28	6.27 ± 0.40	4.56 ± 1.04
3C295	0.460	173.5	166	1548	2.47	0.63	4.99	5.80	1.00	840 ± 66	5.13 ± 0.24	4.52 ± 0.34	2.63 ± 0.66
MACSJ0159.8-0849 .	0.405	27.3	247	2308	1.84	0.69	5.00	23.74	1.00	1324 ± 127	9.59 ± 0.50	9.62 ± 1.01	9.86 ± 3.12
RXJ1347.5-1145	0.451	13.0	116	1821	2.17	0.60	5.00	5.93	3.77	1446 ± 100	14.03 ± 0.69	12.05 ± 0.82	13.83 ± 2.82
MACSJ1621.3+3810	0.461	34.7	263	2059	2.29	0.67	4.96	16.73	1.00	992 ± 71	7.53 ± 0.41	6.42 ± 0.48	4.37 ± 1.01
MACSJ0329.6-0211 .	0.450	26.6	50	466	2.14	0.49	1.59	0.00	1.00	915 ± 83	5.24 ± 0.38	5.23 ± 0.60	3.64 ± 1.02

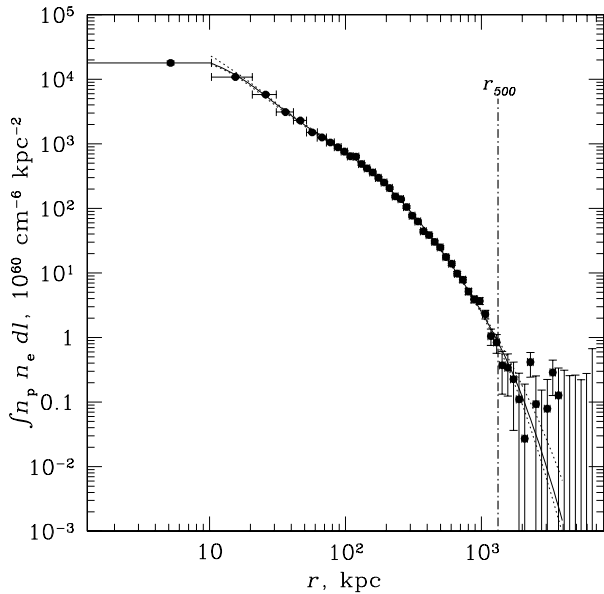[a] The obtained best-fit parameters of the 3D gas density distribution. For definition see Eq.3 in Vikhlinin et al. (2005b)

F . 1.— Observed emissivity profile for MACSJ0159.8-0849. The solid line shows the best-fit profile and the dashed lines correspond to its 68% CL uncertainties

with Galactic absorption. The absorber's hydrogen column density was fixed at values provided by HI radio surveys (Dickey & Lockman 1990). The metallicity was allowed to be free in almost all annuli except the outermost ones, where it was fixed at an average value from the two outermost bins where direct measurements were possible.

The X-ray brightness profiles were extracted from the images in the 0.7–2 keV energy band in concentric annuli with $r_{out}/r_{in} = 1.1$. Using the observed projected temperature and metallicity profiles, the raw *Chandra* counts were converted to the profiles of the projected emission measure, $\int n_e n_p dl$, as described in Vikhlinin et al. (2005b). The profiles from different pointings were added using the statistically optimal weighting. The resulting EM profiles were used to derive the gas density profile.

3. PROFILE MODELING AND DETERMINATION OF THE CLUSTER MASS

The 3-dimensional gas density profile was derived by fitting the observed emission measure profile to a model used by Vikhlinin et al. (2005b) to describe the 3-D gas density distribution in the low-redshift *Chandra* sample (see their equation 3). This function is a modification of the so-called β-model (Cavaliere & Fusco-Femiano 1978), designed to independently fit the gas density slopes in the cluster center, outskirts, and in the intermediate region, and also to allow for an additional emission component in the very central region. The statistical quality of the *Chandra* data for high-z clusters (an example is shown in Fig.1) is sufficient to fit the same set of parameters that Vikhlinin et al. (2005b) used for the low-z clusters. The best-fit parameters of the gas density profiles are listed in Table 1. The projected emission measure corresponding to the best-fit model in MACSJ0159.8-0849 is shown by solid line in Fig.1.

For derivation of the 3-dimensional gas temperature profile we also followed the procedure in Vikhlinin et al. (2005b). Specifically, a model with a great functional freedom was assumed for the 3D profile (see equation 6 in Vikhlinin et al. 2005b). It was projected along the line of sight using the best-fit gas density profile. The projection uses the method that accurately predicts the single-temperature fit for a mixture of plasma spectra with different T (Vikhlinin 2005; Mazzotta et al. 2004). The parameters of the 3D model were obtained by minimizing $\chi 2$ computed using the projected model and observed temperature values at each radius. In some cases, the functional freedom of the 3D model was insufficient to accurately describe the data simultaneously in the very central region and at large radii. In such cases, we excluded several innermost temperature measurements since our prime goal is the mass determination at large radii. The ob-
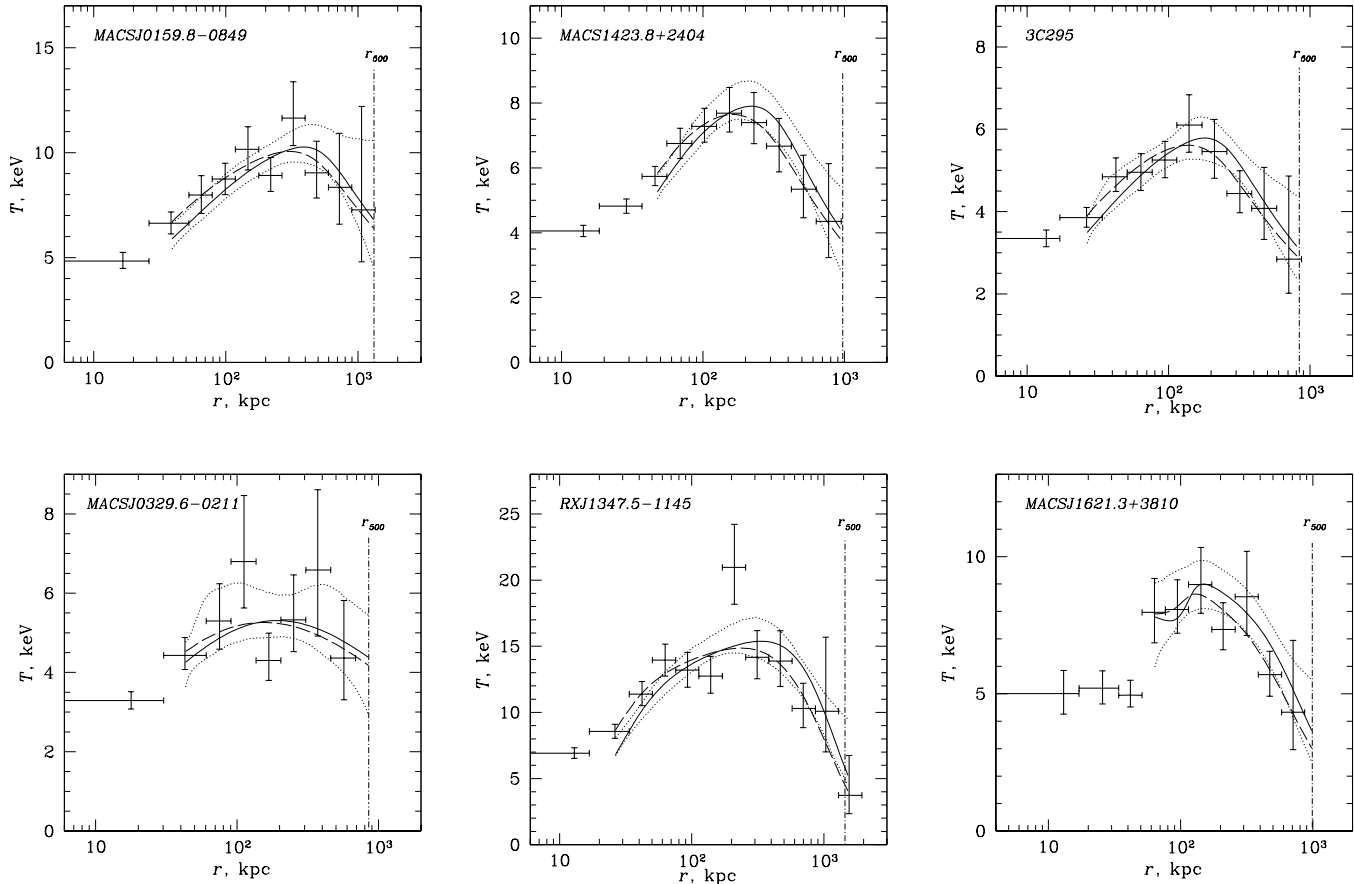
detected in the Southern part of the *Chandra* image and is undetectable in the Northern part. In this case, we excluded the data within the lower (Southern) 50% of the field of view. We also excluded from the analysis the two outermost bins in the MACSJ1621.3+3810 temperature profile because of potential contamination by the foreground emission. In addition, there is a small-scale extended source at RA = 245.296°; Dec = 38.209°, also masked out. The only cluster in our sample that shows some signs of a recent merger is RXJ1347.5–1145 (Allen et al. 2002; Gitti & Schindler 2004). In this case, we masked out the X-ray subclump at $20''$ Southeast of the cluster center. We also excluded the sector PA = $180° − 225°$. This sector shows an excess of the X-ray surface brightness compared to all other directions, which is probably associated with the trail of the merging subcluster.

The three-dimensional gas density and temperature profiles were derived from the azimuthally averaged X-ray brightness and projected temperature profiles centered on the cluster X-ray brightness peak. The projected temperatures were measured using the spectra accumulated in the concentric annuli with $r_{out}/r_{in} = 1.5$. These spectra were fit to the single-temperature MEKAL model (Mewe et al. 1985)

F . 2.— Observed temperature profiles of a sample of distant clusters observed with *Chandra*. The solid lines show the best-fit 3-D temperature profiles and the dotted lines correspond to their 68% CL uncertainties. The dashed lines show the projected best-fit 3-D temperature profiles (2-D). For MACSJ0329.6-0211, we do not show the two outermost temperature bins because they can be contaminated by the foreground emission (see text); these bins were not used in the 3D modeling.

served temperature profiles are shown along with the best fit models in Fig.2.

The total cluster mass profile was derived by direct application of the hydrostatic equilibrium equation (e.g., Sarazin 1988) to the best fit gas density and temperature profiles. The mass profile was used to find the radius corresponding to the mean spherical overdensity $\Delta = 500$ relative to the critical density at the cluster redshifts. The corresponding masses, M_{500}, are reported in Table 1 and the values of r_{500} are indicated in Fig.1 and 2.

Using the best-fit three dimensional profiles, we also computed the average temperatures excluding the central region, as was done in Vikhlinin et al. (2005b) for the low-redshift clusters. We derived the average spectroscopic temperature, T_{spec}, a value obtained from a single-temperature fit to the integrated spectrum, and computed the gas mass-weighted average T_{mg}, both in the 70 kpc–r_{500} radial range. These averages were used by Vikhlinin et al. (2005b) to derive the $M-T$ relations for nearby clusters and therefore we can use their results as the low-redshift reference.

All the essential parameters derived from the 3-dimensional modeling are reported in Table 1. The parameter uncertainties were estimated by the Monte-Carlo simulations technique described in § 3.3 and 3.4 of Vikhlinin et al. (2005b).

4. $M - T$ RELATION

TABLE 2
P   L   F   C   *Chandra*
XMM-Newton M   -T   R

Temperature average	α	γ
T_{spec}.............	1.02 ± 0.20	1.55 ± 0.14
T_{mg}..............	1.33 ± 0.20	1.65 ± 0.15

N   . — Parameters γ characterize the slope of the $M - T$ relation, $E(z)M_{500} \propto T^{\gamma}$, and evolution in its normalization, $M_{500}/T^{3/2} \propto E(z)^{-\alpha}$. See text for details.

Figure 3 shows the derived $M-T$ relation for $z > 0.4$, which combines the *XMM-Newton* results from Kotov & Vikhlinin (2005) and the *Chandra* results described here. There is clearly a good overall agreement between the two datasets. There is a small difference in our modeling procedure for the *XMM-Newton* and *Chandra* data (we used more restrictive models for $\rho_g(r)$ and $T(r)$ to fit the *XMM-Newton* data). However, we checked that this difference results in a negligibly small offset in the mass estimates. Applying the more restrictive models that were used in the *XMM-Newton* analysis to the *Chandra* data, we obtain that the derived values of M_{500} change by 3% on average.

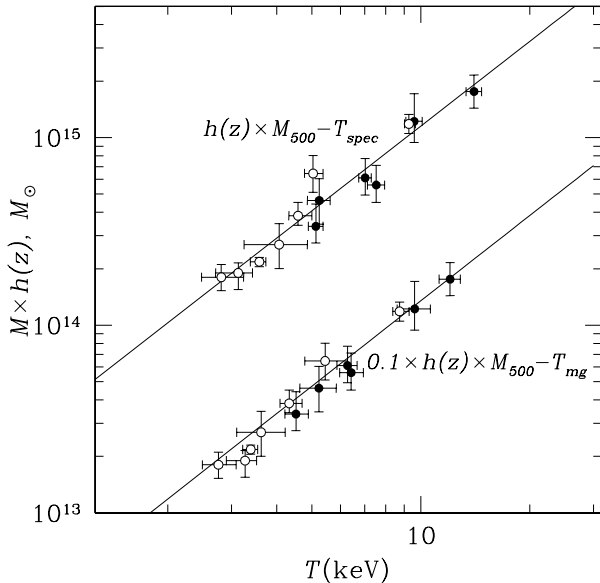To quantify the high-redshift $M - T$ relation, we model

F . 3.— Correlation of $M - T_{spec}$ (the upper-left corner) and $M - T_{mg}$ (the lower-right corner) at r_{500} for the combined *XMM-Newton*(open circles) and *Chandra*(solid circles) sample. The solid lines show the low-redshift results from Vikhlinin et al. (2005b).

separately the evolution in normalization and the slope of de-evolved relation. The evolution in the normalization is parametrized as $M_{500}/T^{3/2} \propto E(z)^{-\alpha}$, where the low-redshift normalization is fixed at the *Chandra* measurements by Vikhlinin et al. (2005b). The joint fit to the *Chandra* and *XMM-Newton* results for distant clusters gives $\alpha = 1.02 \pm 0.20$ and $\alpha = 1.33 \pm 0.20$ for the $M - T_{spec}$ and $M - T_{mg}$ relations, respectively[3] (see also Table 2). These values are close to, and consistent with, the expected self-similar evolution, $\alpha = 1$.

Assuming that the normalization of the $M - T$ relation indeed evolves self-similarly, we can "de-evolve" each mass

[3] Uncertainties include that for the normalization of the low-z mass-temperature relations from Vikhlinin et al. (2005b).

measurement using the correction factor $E(z)$ and fit the slope in the high-redshift $M - T$ relation, $E(z)M_{500} \propto T^{\gamma}$. For the $M - T_{spec}$ and $M - T_{mg}$ relations we measure slopes of $\gamma = 1.55 \pm 0.14$ and $\gamma = 1.65 \pm 0.15$, respectively (see also Table 2). These values are also close to the predictions of the self-similar theory, $\gamma = 3/2$, and to the low-redshift measurements (Vikhlinin et al. 2005b; Arnaud et al. 2005).

5. CONCLUSIONS

Deep *Chandra* and *XMM-Newton* observations of relaxed clusters at $z > 0.4$ provide direct hydrostatic mass measurements at the critical overdensity level $\Delta = 500$. The resulting determination of the high-redshift $M - T$ relation is comparable to the low-redshift studies both in terms of the sample size and mass measurement uncertainties for individual objects.

We find that the $M - T$ relation at $z = 0.4 - 0.7$ is consistent with the self-similar evolution of that for low-redshift clusters. Parametrizing the evolution of the normalization as $M/T^{3/2} \propto E(z)^{-\alpha}$ we measure α close to 1 (Table. 2). The de-evolved relation, $E(z)M - T$, has the power law slopes close to $\gamma = 1.5$ (Table 2). This is an important confirmation of one of the key predictions of the cluster formation theory (Eke et al. 1996; Bryan & Norman 1998) and also a welcome news for cosmological interpretation of the cluster number density measurements at $z > 0$.

We should caution, however, that our results are based on the data for highly relaxed clusters, which represent only a fraction of the total population, especially at high redshifts. Extrapolation of the observed $M - T$ relation on the entire population requires further studies with the help of numerical simulations and independent mass measurements from gravitational lensing.

REFERENCES

Allen, S. W., Schmidt, R. W., & Fabian, A. C. 2002, MNRAS, 335, 256
Allen, S. W., Schmidt, R. W., Ebeling, H., Fabian, A. C., & van Speybroeck, L. 2004, MNRAS, 353, 45
Arnaud, M., Pointecouteau, E., & Pratt, G. W. 2005, A&A, 441, 893
Bryan, G. L., & Norman, M. L. 1998, ApJ, 495, 80
Cavaliere, A., & Fusco-Femiano, R. 1978, A&A, 70, 677
Dickey, J. M., & Lockman, F. J. 1990, ARA&A, 28, 215
Eke, V. R., Cole, S., & Frenk, C. S. 1996, MNRAS, 282, 263
Ettori, S., Tozzi, P., Borgani, S., & Rosati, P. 2004, A&A, 417, 13
Gitti, M., & Schindler, S. 2004, A&A, 427, L9
Kotov, O., & Vikhlinin, A. 2005, ApJ, in press, (astro-ph/0504233)
Markevitch, M., & Vikhlinin, A. 1997, ApJ, 491, 467
Markevitch, M., et al. 2003, ApJ, 583, 70
Mathews, W. G. 1978, ApJ, 219, 413
Maughan, B. J., Jones, L. R., Ebeling, H., & Scharf, C. 2005, mnras, accepted for publication (astro-ph/0503455)

Mazzotta, P., Rasia, E., Moscardini, L., & Tormen, G. 2004, MNRAS, 354, 10
Mewe, R., Gronenschild, E. H. B. M., & van den Oord, G. H. J. 1985, A&AS, 62, 197
Sarazin, C. L. 1988, Cambridge Astrophysics Series, Cambridge: Cambridge University Press, 1988,
Vikhlinin, A., McNamara, B. R., Forman, W., Jones, C., Quintana, H., & Hornstrup, A. 1998, ApJ, 502, 558
Vikhlinin, A., Markevitch, M., Murray, S. S., Jones, C., Forman, W., & Van Speybroeck, L. 2005a, ApJ, 628, 655
Vikhlinin, A., Kravtsov A., Forman, W., Jones, C., Markevitch, M., Murray, S. S., & Van Speybroeck 2005b, ApJ submitted, (astro-ph/0507092)
Vikhlinin, A., 2005, ApJ, submitted, (astro-ph/0504098)
Voit, G. M. 2005, Reviews of Modern Physics, 77, 207